Transient lateral photovoltaic effect in patterned ferromagnetic metal-oxide-semiconductor films

Isidoro Martinez[a], Juan Pedro Cascales[a], Antonio Lara[a], Pablo Andres[a] and Farkhad G. Aliev[a]

[a] Dpto. Fisica de la Materia Condensada C-III, Instituto Nicolas Cabrera (INC) and Condensed Matter Physics Institute (IFIMAC), Universidad Autonoma de Madrid, Madrid 28049, Spain

ABSTRACT

The time dependent transient lateral photovoltaic effect (T-LPE) has been studied with microsecond time resolution and with chopping frequencies in the kHz range, in lithographically patterned 21 nm thick, 5, 10 and 20 micron wide and 1500 micron long Co lines grown over naturally passivated p-type Si (100). We have observed a nearly linear dependence of the LPE transient response with the laser spot position. An unusual T-LPE dynamic response with a sign change in the laser-off stage has also been corroborated by numerical simulations. A qualitative explanation suggests a modification of the drift-diffusion model by including the influence of a local inductance. In addition, influence of anisotropic magnetoresistance of the Co line structure on dynamic response on T-LPE has been investigated. Specifically, we have experimentally investigated influence of the direction of the external magnetic field respect to the drift velocity of the photogenerated carriers on the T-LPE. We have observed notable dependence of the T-LPE on the magnetic field in the small field range (below 100 Oe), compatible with anisotropic magnetoresistance values. The strong influence of the magnetization alignment on the dynamic response of photogenerated carriers has been also observed through a phase sensitive lock-in experiment. These findings indicate that the microstructuring of the ferromagnetic line based position sensitive detectors (PSD) could improve their space-time resolution and add capability of magnetic field tuning of the main PSD characteristics.

Keywords: Lateral photovoltaic effect, Dynamic response, Lithographically patterned structures, Anisotropic Transient Lateral Photovoltaic effect

1. INTRODUCTION

Non-uniform illumination of the semiconductor surface or ultrathin metallic films forming Metal - Oxide - Semiconductor (MOS) structures generates an electric fields parallel to the surface or to the Schottky barrier due to photocarrier drift in non-equilibrium conditions. The straight-forward way to maximize the potential difference is to generate photo-carriers effectively (by using laser with photon energy exceeding the gap) with spot diameter much less than the distance between the laterally situated contacts. This potential difference is known as the lateral photovoltaic effect (LPE).[1–4] Since a few decades, the LPE has been reported in wide classes of systems ranging from organic semiconductors,[5] Ti/Si amorphous superlattices,[6] semiconductor heterostructures,[7] including two-dimensional electron systems (2DES).[8] On the practical side, the LPE has been widely used to develop high precision position-sensitive detectors (PSD).[9–11] Among the main challenges for LPE based devices there is optimizing their spatial sensitivity and reaction time. So far the main root to increase spatial sensitivity of the LPE based PSDs has been achieved by the use of metal-semiconductor junctions, and quite recently metal-oxide-semiconductor junctions (MOS) with different types of metals (Ti, Co, ...)[6,12] Interestingly, both kinetic parameters: resistance and lateral photovoltaic effects could be affected similarly by an external magnetic field. Indeed, a certain correlation has been reported between magnetoresistance and LPE in $Co_3Mn_2O/SiO_2/Si$ structures.[13] This points out the possibility to tune the LPE by using the ferromagnetic properties of metallic layers in MOS strutures.

Further author information:
Farkhad G. Aliev: E-mail: farkhad.aliev@uam.es

Physics, Simulation, and Photonic Engineering of Photovoltaic Devices IV, edited by Alexandre Freundlich, Jean-François Guillemoles, Masakazu Sugiyama, Proc. of SPIE Vol. 9358, 93580O · © 2015 SPIE
CCC code: 0277-786X/15/$18 · doi: 10.1117/12.2079071

The particular interest shown in $Co/SiO_2/Si$ structures is related to the possibility of developing broadband PSD for the visible, ultraviolet or infrared range[14–16] by adjusting the Co thickness. Previous studies of MOS structures, including $Co/SiO_2/Si$, investigated the LPE by illuminating steadily a relatively large rectangular samples (about $10\times10\ mm^2$). A laser beam of a few mW was typically focused onto a 10-50 μm spot and the open circuit LPE was measured between two contacts which extended along opposite edges.[10,14,16] In wide devices, the dynamic response is dominated by the barrier capacitance which results in a unipolar (charge-discharge type) response[17] which diminishes in amplitude when the chopper frequency approaches the kHz range.[18] Moreover, the steady state LPE value diminishes substantially when the Co thickness approaches 20 nm.[12]

Recent advances in electron beam lithography have permitted the development of MOS structures where the LPE can be investigated along patterned, micron wide, metallic line structures. The time dependent photovoltaic response along such structures might be different from the one observed in the wide LPE devices. Here we investigate the lateral photovoltaic effect in lithographically patterned (21 nm thick, 5, 10 and 20 μm wide and 1500 μm long) Co lines with or without external magnetic field. The structures were deposited on a naturally passivated (about 2 nm SiO_2) Silicon (100) substrate. More details on preparation and characterization of samples may be found in.[19,20] We have studied the transient photovoltaic effect (T-LPE)[4,21,22] as a response to turning the laser beam illumination ON (steady state, referred to as the ON state) followed by switching the laser OFF (decaying regime, referred to as the OFF state) as a function of the spot position, pulse frequency and power. We observe peak-like transitorials which present a sign inversion of the T-LPE in the OFF state followed by a nearly exponential relaxation back to equilibrium. We have corroborated this behavior of the T-LPE response with numerical simulations. We have qualitatively explained the results with a simple model which takes into account the local inductance of the metallic line structure deposited on top of a Schottky barrier. We observe a substantial increase of the position sensitivity of patterned line structures when their width is reduced, measured by the peak to peak response. Preliminary results related to this part which were reported by Cascales et al.[23] have been expanded and detailed in the present manuscript. In addition, we report on the substantial influence of the magnetic state on T-LPE and link it with the anisotropic magnetoresistance (AMR) of Co films. In order to vary AMR values we cover the Co line structures with thin Au layer which change both resistance and magnetoresistance of the structures keeping the remaining parameters (Schottky barrier) intact. Numerical simulations confirm a direct link between AMR and T-LPE. The influence of the magnetic state of the ferromagnetic overlayer on the LPE has been additionally confirmed via phase sensitive lock-in measurements.

2. EXPERIMENTAL METHODS

We have investigated the T-LPE effect with two different experimental setups, using a voltage digitizer card or a lock-in amplifier. Since the patterned structures of our PSDs include a ferromagnetic overlayer, we have also investigated the possible effect of a magnetic field on the T-LPE. The main experimental techniques, in the presence of an external applied magnetic field are detailed below.

2.1 Real time T-LPE measurements

The optical setup depicted in Fig. 1(a) comprised of a microscope objective lens (MO) (50x, 0.42 NA, Plan APO, working distance 21 mm) that focuses the laser beam into the sample. The image of the sample is relayed into a CCD camera by using the objective and a beam splitter. The potential difference created along the line is measured from three pairs of $500\times500\ \mu m^2$ Cobalt pads which are contacted with gold wires by using indium. The transient LPE has been studied by applying a train of periodic laser beam pulses. TOPTICA-iBeam Smart diode lasers which emit light of 405 or 487 nm of wavelength λ have been used. The optical setup is common to both detection methods.

The T-LPE signal between contacts is amplified in two stages. The first stage is a home-made low noise preamplifier (bandwidth from DC to 1 MHz) with a maximum gain of 47, then is followed by a low noise SR750 amplifier with a tunable gain and filter bandwidth. Depending on the roll-off frequency of the amplifier filter, the detection of the fast "laser off" transition can be affected, as was shown elsewhere.[23] The voltage, amplified up to 10^5 times, was measured using a NI-PCI 5922 digitizer which works at frequencies up to 2MHz. The square wave used to modulate the laser pulses was supplied by a Keithley K6221 current source. A number of

experimental parameters were controlled by computer software, such as the sample motion (via Zaber T-L-A linear actuator), the frequency of the pulses, the power of the laser beam and data acquisition.

We have also studied the effect of an in-plane magnetic field, applied perpendicular to the Cobalt line, on the T-LPE signal. The samples have been placed in the midst of two Helmholtz coils so the external magnetic field is applied as is schematically shown in Fig. 1.

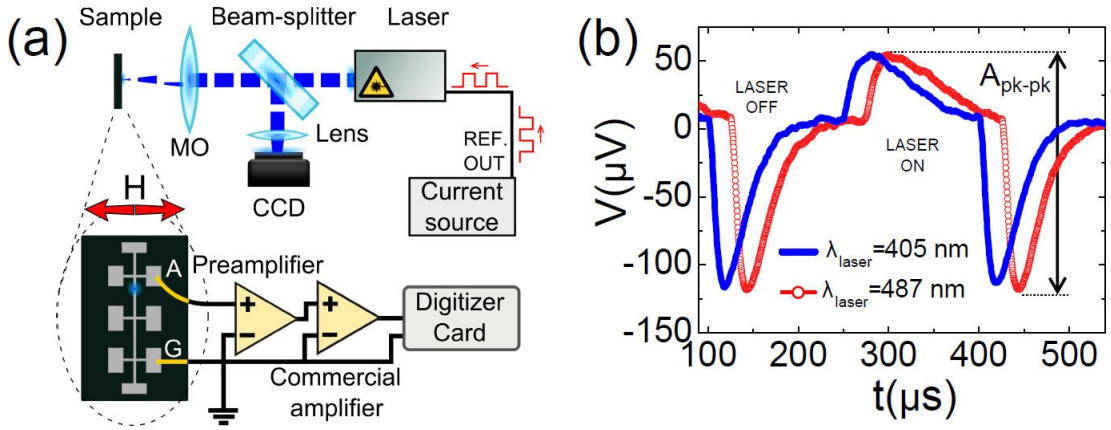

Figure 1. (a) Diagram of the experimental set-up. (b) Time dependent LPE with f=3.33 kHz and P=0.76mW for a 10 μm Co line for light pulses with wavelengths of 405 nm and 487 nm.

An example of the T-LPE response when the device is subjected to a periodically modulated light beam can be seen in Fig. 1(b), where the T-LPE response shows peak-like transitorials presenting a sign inversion in the OFF state. The OFF state peak is followed by a nearly exponential relaxation back to equilibrium. The nearly exponential characteristic relaxation time τ_{OFF} will be discussed further below.

We will refer to the time-dependent periodic signal as a *timeserie*. The timeseries, measured for every position of the laser spot, contain a few hundred periods of the reference signal, and the signal is averaged to obtain an average response for only period. From the averaged T-LPE at every position we obtain the voltage of the positive peak and the negative peak and their difference gives us the peak to peak amplitude of the signal. This is the key experimental parameter in this method we are going to analyze further on.

Since the band gap of Silicon is of 1.11 eV, illuminating our devices with wavelengths from 400 to 700 nm is effective in exciting electrons from the valence to the conduction band. The photogenerated current should increases with the wavelength of the light used. Qualitatively similar T-LPE measurements were obtained for two different light wavelengths. A further improvement of the position sensistivity could be obtained by using a laser in the infrarred range.[16] In Fig. 1(b) we show that the T-LPE response does not change appreciably if 405 or 487 nm light is used. All the experimental data shown from now on has been measured with the 487 nm laser.

2.2 Lock-in detection method

Under conditions of periodic light modulation with frequencies around a few kHz, the amplitude and the phase of the response of the system may be used to characterize the lateral photovoltaic effect in MOS-type PSDs.[9] The phase of the photovoltage has been used as alternative, high precision detection method of the position of a signal.[24] The main advantage of such a method is related with its insensitivity to the variation of the incident light intensity. Here we use a similar techique which additionally incorporates the possibility to determine LPE phase changes both as a function of position and of value of the external magnetic field.

Our lock-in setup is quite straight-forward, and consists on modulating the amplitude of the incident beam with a reference signal provided by the lock-in amplifier. The LPE voltage is then input into the lock-in and

the magnitude and phase of the voltage at the reference frequency is registered. A diagram of the experimental setup is shown in Fig.2(a).

As can be seen in Fig. 2(b), the voltage depends linearly on the position of the laser spot (typical LPE behaviour). If we take the phase θ at the beggining of the device ($X = 0$) as the reference, then the phase of the signal can be seen to deviate from 0 as the laser spot moves away from the positive electrode. This change in phase is due to the change in distance that the signal has to travel to reach the electrode as the laser spot is moved. Measuring the phase instead of the voltage has already been proposed for PSD sensors,[9] as the voltage may be more sensitive to external variations while the phase remains more robust as a function of the position. Even though our sample has a total length of 1.5 mm, the dependence of the phase on the position presents a similar behaviour as in Ref.[9] (where the sample size is of the order of a cm), although the total phase change of around 60 ° is somewhat smaller.

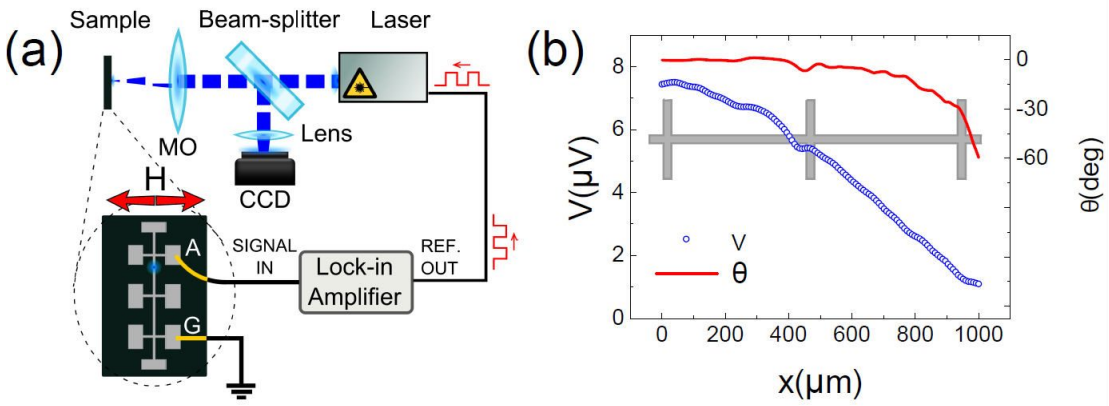

Figure 2. (a) Diagram of the lock-in experimental setup. (b) Voltage and phase of the LPE signal registered by the lock-in for different laser spot positions.

If an in-plane external magnetic field is applied, a change in the phase of the signal may be seen when the magnetization of the Co line is inverted. Results regarding this matter and a discussion of the observed effect are shown further below.

3. EXPERIMENTAL RESULTS IN THE ABSENCE OF A MAGNETIC FIELD

This section presents T-LPE measurements comparing 5 μm, 10 μm and 20 μm wide Co line structures grown over naturally passivated p-type Si(100) substrates. The voltage values discussed here correspond to the peak to peak amplitude of the T-LPE signal. Figures 3(a-c) analyze the influence of the laser power P on the peak to peak ($pk - pk$) voltage in 5 μm, 10 μm and 20 μm wide lines. The laser power that reaches the sample after the optical circuit is estimated from irradiance measurements. As can be seen in Fig. 3(d), the $pk - pk$ T-LPE amplitude is higher for narrower lines, and it increases gradually with the laser power, reaching a maximum at around $P = 5.5\ mW$ and then abruptly decreases. This behavior could be explained by the enhancement of a $p - n$ recombination probability when the concentration of photogenerated carriers is highest. We note that the observed T-LPE inversion remains qualitatively unchanged with the variation of the laser power in the investigated range, for all Co widths.

As is shown in Fig. 4(b) of the article, the $pk - pk$ amplitude can be improved significantly as the Co line is made narrower, which reflects on the narrowest sample have a higher spatial sensibility.

We have also studied the effect of a 12 nm gold coating on the T-LPE in MOS devices. The gold coated samples show the same linear behaviour of the T-LPE signal as a function of the laser position. The addition of the coating reduces the resistance of the line structure, while it enhances de absorption of light, producing a reduction of the T-LPE signal amplitude (see Fig. 7).

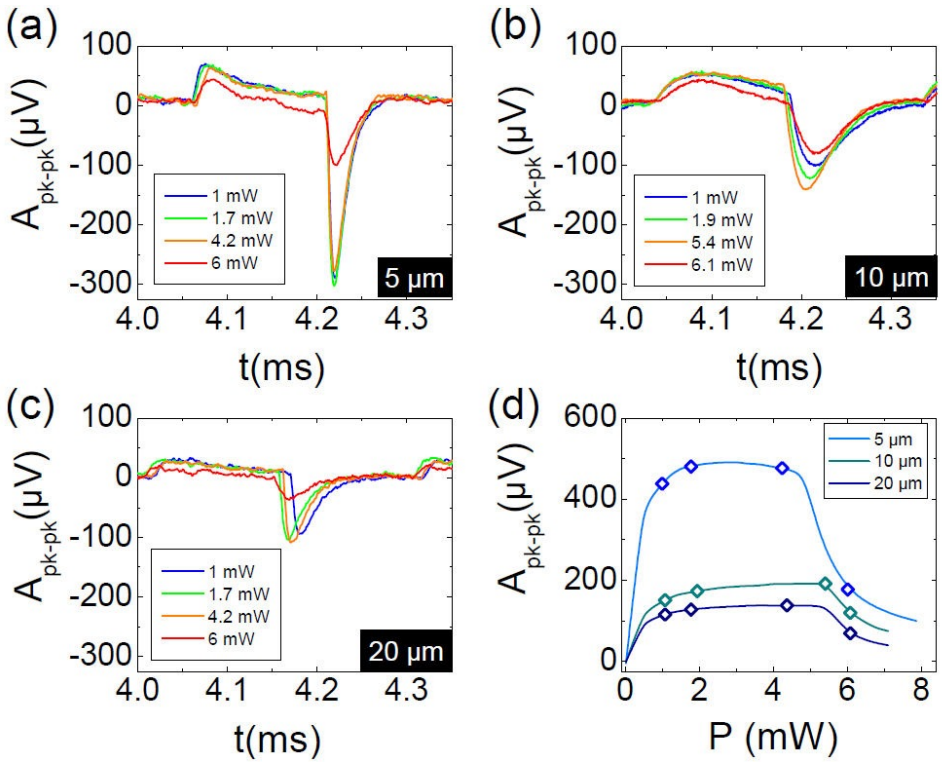

Figure 3. Change of the T-LPE response with the applied laser power for (a) 5 μm, (b) 10 μm and (c) 20 μm wide Co lines. (d) $pk-pk$ amplitude as a function of the laser power for 5 μm, 10 μm and 20 μm Co lines. Open dots indicate correspond to the graphs (a)-(c).

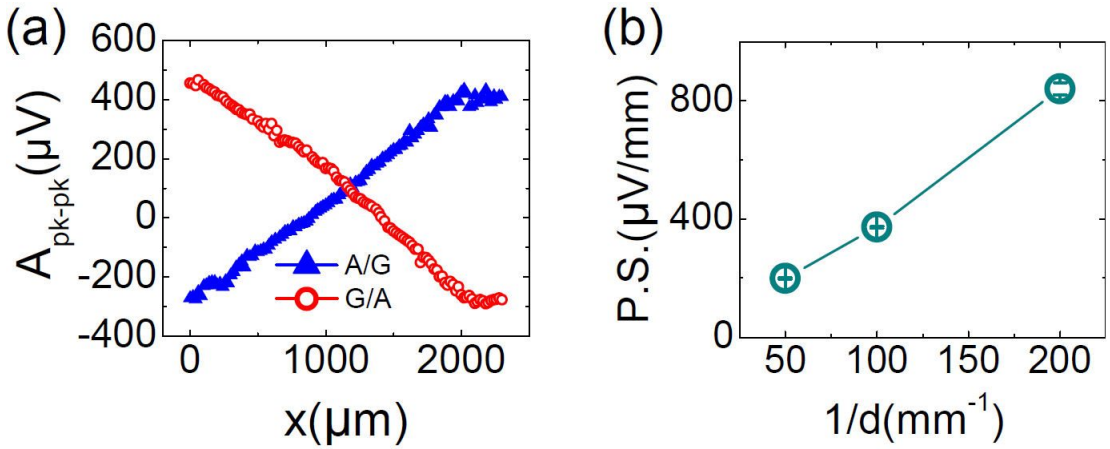

Figure 4. (a) Dependence of the signal amplitude with the position X, for two electrode configurations, showing a typical LPE linear behaviour. (b) Dependence of the resistance and position sensitivity with $1/d$, with d the Co line width.

In general, we observe that in between the electrodes, the LPE amplitude varies linearly with the spot position Fig. 4, the most important feature of planar LPE devices.[1–4] This behavior is independent of the contact configuration with respect to the ground. It is worth noting that the T-LPE amplitude and shows a non-zero value when spot is centered exactly between the electrodes. This is discussed in the following section.

3.1 ANALYTICAL MODEL OF THE T-LPE IN MOS PATTERNED LINES

In a previous publication,[23] we were able to reproduce qualitatively both the linear dependence and the offset at non-zero offset of the T-LPE amplitude by using a one dimensional drift-diffusion model[1,2] which calculates the stationary potential distribution and potential difference employing two different (Robin / 3-rd type) boundary conditions. We have also described the peak-like T-LPE and its sign inversion in the off state by adding a term to the equation for the dynamic T-LPE response in wide two-dimensional structures.[1,2] This new term corresponds to the local inductance L of our metallic wire. The resulting equation is thus:

$$A\frac{d^2u(x,t)}{dt^2} + B\frac{du(x,t)}{dt} - D\frac{d^2u(x,t)}{dx^2} + Eu(x,t) = F(x,t) \tag{1}$$

where $A \propto L, C$, $B \propto R, C$, the relation between terms D and E describes the carrier diffusion along the device and F corresponds to the electron-hole separation function.

As can be seen in Fig. 5(a), by shifting the position of the charge source x_L, the amplitude of the position dependent model depends linearly on x and is non-zero at $x = L/2$.

The time dependent solution of equation (1), at a fixed x_0, corresponds to the driven harmonic oscillator equation, or a RLC circuit:

$$L\frac{d^2u(x_0,t)}{dt^2} + R\frac{du(x_0,t)}{dt} + \frac{1}{C}u(x_0,t) = F(x_0,t) \tag{2}$$

The model presents an excellent agreement with the experimental results, as shown in Figure 5(b), for the case when equation 1 describes an underdamped oscillator very close to the overdamped regime.[23] Using the resistance of the 10 μm Co line, we obtain an estimate of the capacitance and inductance of the strip from the fit. The resistance of the 5 μm sample is twice that of the 10 μm strip, and using as capacitance half of what was obtained for the 10 μm sample, we obtain values of inductance which are 60 % higher.[23]

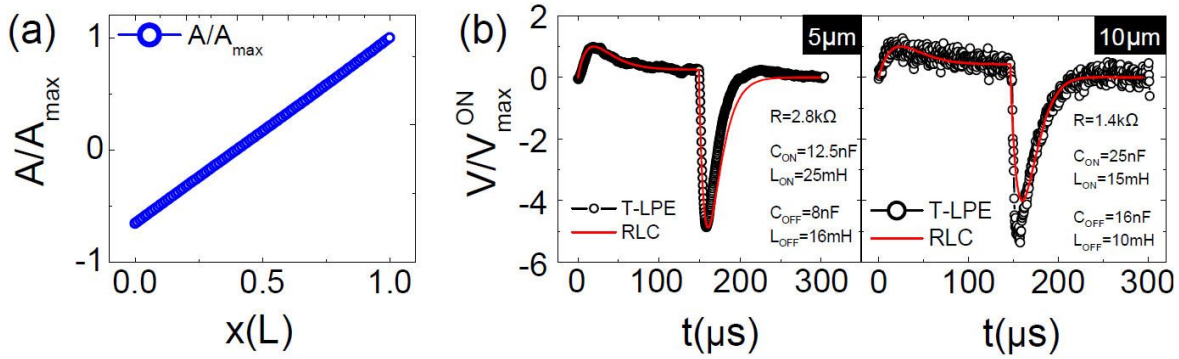

Figure 5. (a) Position-dependent solution of the model, with x_0 the laser spot position and the constants B = 1; F = 1;E = 1;D = 3;L = 1; h = 0:6; s = -1. (b) Comparison of an T-LPE response in 5 μm and 10 μm wide Co lines with the driven RLC circuit (equation (2)).

4. ANISOTROPIC MAGNETORESISTANCE VERSUS ANISOTROPIC TRANSIENT LATERAL PHOTOVOLTAIC EFFECT

The effect of an external magnetic field on the T-LPE has also been studied. As shown in Fig. 1(a), the magnetic field was applied in plane and perpendicular to the direction of the Co line. We carried out field cycles from a positive saturation value down to a negative saturation value (back branch), and back to the positive saturation field (forth branch).

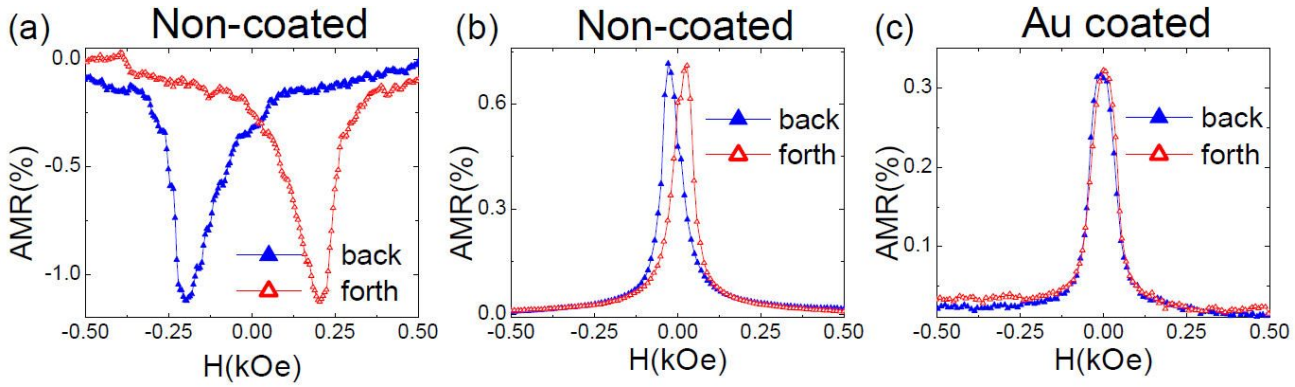

Figure 6. Anisotropic magnetoresistance comparison for a 10μm wide Cobalt lines: (a) parallel to the line, (b) perpendicular to the line and (c) perpendicular to the line (gold coated Co). The normalization has been made by subtracting A_{pk-pk}(1 kOe).

Resistance measurements as a function of an in plane field, both along the direction of the Co line and perpendicular to it reveal anisotropic magnetoresistance (AMR) effects. Only fields perpendicular to the Co line structure are discussed here. The AMR of the Cobalt line was found to present a peak at low fields (around 20-30 Oe), with a maximum AMR ratio of 0.6% as can be seen Fig 6. This is a well-known effect in ferromagnets when the local magnetization interacts with an electron current, depending on the relative angle between the local magnetization and the direction of the current.

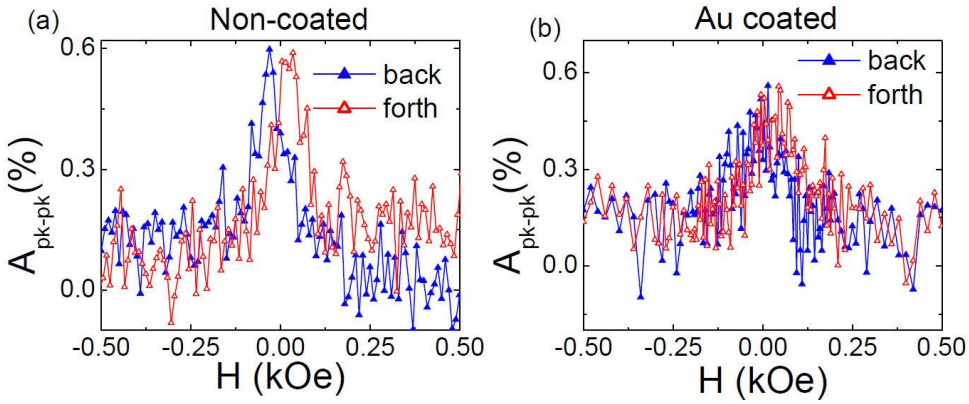

Figure 7. Anisotropic lateral photovoltaic effect comparison for a 5μm Cobalt line width with (a) no coating and (b) gold coated. The normalization has been made subtracting the 1kOe value.

We have found that the T-LPE amplitude is enhanced by 0.6% (see Fig 7), at fields which correspond to the maximum in AMR of the Co line devices. We define this effect as Anisotropic Transient Lateral Photovolatice Effect (A-T-LPE). If the MOS system is coated with gold, the absolute values of the A-T-LPE are reduced almost by half due to the increment of absorbed light and the previously mentioned increment of conductance. A-T-LPE results for 5μm and 10μm Cobalt line widths are similar. These observations indicate that the T-LPE

variation with an applied magnetic field is directly related with anisotropic magnetoresistance. We support this conclusion by micromagnetic simulations and numerical simulations (see Fig. 11).

4.1 Influence of an external magnetic field on the T-LPE relaxation times

The application of an external magnetic field has been found also to influence the relaxation time of the laser OFF transition discussed above. Figure 8(a) presents an analysis of τ_{OFF} *vs.* H for a full field cycle. The relaxation time τ_{OFF} was obtained by fitting an exponentially decaying function to the decaying part of the OFF peak (not shown for brevity). As can be seen, the relaxation time for negative fields is noticeably lower than for positive fields, and a step-like transition between both regimes is seen close to the switching field of the Co line known from AMR measurements.

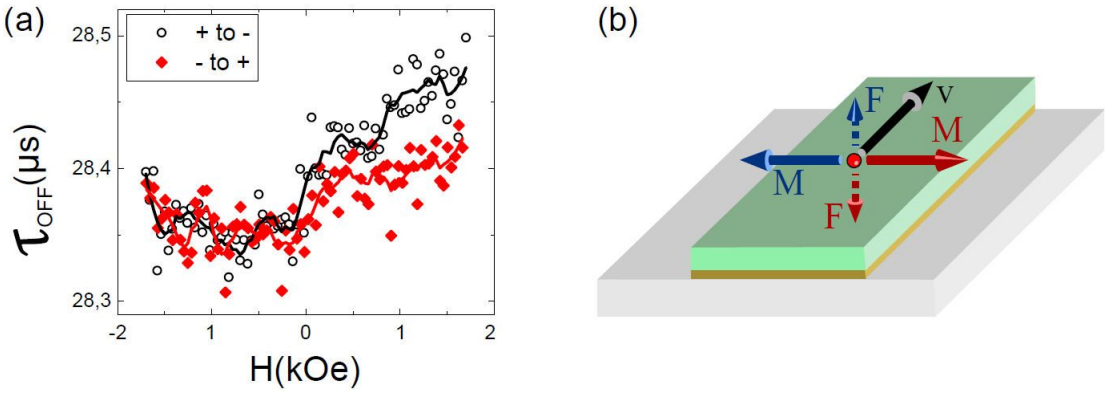

Figure 8. (a) Dependence of the laser OFF relaxation time on the external magnetic field for a 10 μm Co line. (b) Diagram representing inversion of the Lorentz force acting over photocarrier due to inversion of the magnetization of ferromagnet

This behaviour may be qualitatively explained by the toy model shown in Fig. 8(b). For a fixed direction of the velocity of the charge carriers, depending on the direction of the applied field, the resulting Lorentz force may shift the carriers upwards or downwards. If the magnetic field forces the carriers downwards, this will promote the recombination processes, accelerating the decay of the our laser OFF peak. Conversely, if the recombination process is delayed becase the carriers remain in the Co for a longer time, τ_{OFF} will increase. We should note that the branches do not meet at the starting point (positive saturation field). This is due to the fact that the measurements take a considerable amount of time to carry out (a few hours), and the temperature conditions could change during the measurement.

5. LOCK-IN METHOD RESULTS

We will now discuss the main results obtained with the lock-in setup, in the presence of an external magnetic field. As was shown in Fig. 2, in the absence of a magnetic field, the voltage presents a typical LPE linear dependence on the position of the laser spot while the phase of the signal varies as the laser spot moves away from the positive electrode because of the diference in distance the signal has to cover.

We have studied the dependence of the voltage and phase on the position in the presence of an external magnetic field. As can be seen in Fig. 9(a) and (b), the voltage amplitude presents a close to linear dependence on the position (consistent with the T-LPE) while an abrupt change in the phase occurs for fields close to the field where the Co lines exhibit an AMR peak (Fig. 6). We have subtracted the phase values for every position for the positive saturation field (right row of the plots), in order to observe only the variation with the field. This behaviour has been consistently observed in our samples. We attribute this effect to the effect of the Lorentz force arising from the local magnetization discussed above (see Fig. 8(b)).

As can be seen, the change in voltage due to the magnetic field within less than 3%, while the change in phase is of around 25°. We mentioned earlier that measuring the phase in PSD sensors has already been proposed.[9] Our results prove that gauging the effect of an external magnetic field on the LPE in a ferromagnetic patterned line is much more sensitive, when a lock-in amplifier is used, if the phase is considered instead of the voltage.

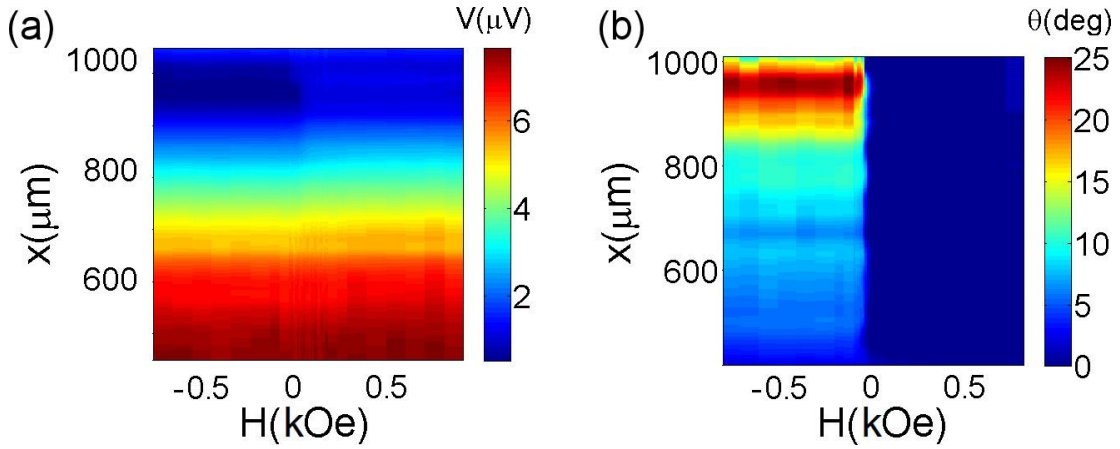

Figure 9. (a) Amplitude and (b) phase of the signal registered by the lock-in. The phase at the saturation field has been subtracted for every spot position for clarity.

6. NUMERICAL SIMULATIONS WITH ATLAS

Our numerical simulations using the ATLAS software, with adjusted parameters and a wavelength $\lambda = 405nm$ have reproduced qualitatively the main experimental findings obtained without a magnetic field, as can be seen in Figure 10. The main simulation parameters which resulted in the best fit to the experiment are shown below.

In order to carry out simulations we build first a two dimensional layer system simulating the real sample layers. We have used a 21 nm thick and $1500\mu m$ long Cobalt layer with two Cobalt contacts on top, at each end of the line to determine the potential difference. Below this layer we situate a 2 nm thick SiO_2 layer followed by a $250\mu m$ thick layer of Silicon.

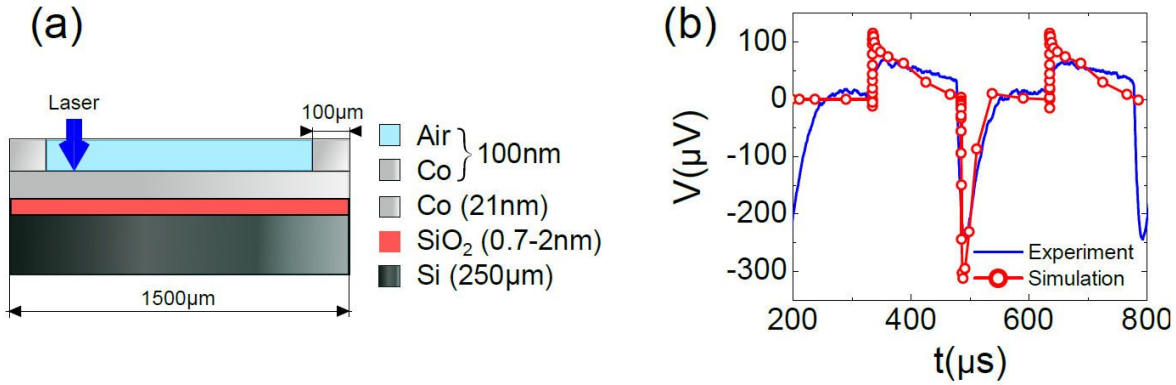

Figure 10. (a) Sketch of the simulated layered structure with the different beam shapes. (b) Comparison between the experiment and simulations of a Co layer on SiO2-Si with a uniform beam. The parameters used are: concentration of doping carriers in Si; n-type $= 10^{13}cm^{-3}$ and p-type $= 2 \times 10^{13}cm^{-3}$; carrier's lifetimes $\tau_p = 2 \times 10^{-5}$ s; $\tau_n = 10^{-6}$ s; Si electrical resistivity $\rho = 16$ $\mu\Omega \times cm$. A Gaussian laser source was chosen with an irradiance $I = 1600$ W/cm^2, $\lambda = 405$ nm and a modulating frequency of $f = 3.33$ kHz.

We consider a Gaussian-shaped laser beam with a diameter of $5\mu m$ focused on top of the first Cobalt layer and near one of the contacts. It is necessary to specify the models that describe the physical system. We can separate them in 5 groups:

1. The carrier statistics model for calculating the number of carriers within the semiconductor due to temperature. It is not specified in the program so ATLAS uses Boltzmann statistics by default.

2. Regarding the mobility model, we use the Lombardi CVT model which is specific for metal-oxide semiconductor devices and takes into account the carrier scattering at material interfaces. This is very important in our experiment because there is a depletion zone provoking charges to move in a very narrow area close to the oxide surface where scattering is a major effect.
3. Recombination model. We use the Shockley-Read-Hall (SRH) model which is recommended for indirect band gap semiconductor.
4. Our simulations also make use of an impact ionization model. In semiconductors there are free electrons that while moving have some chance of colliding with electrons from the valence band making them jump to the conduction band creating an electron-hole pair. There are several models to describe this but as it is not an important process in our case we are not taking this into account.
5. Tunneling and carrier injection models. We use the Fowler-Nordheim tunneling model and for taking into account the carrier injection we apply the Lucky-Electron Hot Carrier Injection Model, which proposes that an electron is emitted into the oxide by first gaining enough energy from the electric field in the channel to surmount the insulator/semiconductor barrier.

We attribute some differences between the experiment and simulation to the capacitance of a real sample as well as the influence of the pre-amplifier, absent in the simulations. In order to check if the observed effects are specific to MOS structures, we have also simulated the T-LPE under the same conditions by decreasing the SiO_2 layer thickness (or removing it altogether). When we remove both SiO_2 and Co layers and leave only the laterally contacted Si surface, the transient LPE response of the pure Si substrate shows an exponential increase (decrease) when the laser is switched ON (OFF), not shown for brevity.

7. NUMERICAL SIMULATIONS WITH THE POISSON EQUATION

Simulation of AMR curves

In order to simulate AMR curves it is necessary to know the electric current and the magnetization distributions. The latter has been obtained with OOMMF,[25] using the following paramenters: magnetic damping $\alpha = 0.1$, exchange stiffness $A = 1.4 \times 10^{-11}$ J/m and saturation magnetization $M_S = 1.4 \times 10^6$ A/m.[26] As for the current, it has been calculated by solving Laplace's equation for the desired geometry. With boundary conditions $V = V_1$ and $V = V_2$ at the two ends of the line, and dV/dn=0 (perpendicular to the boundary) at the rest of the boundaries, we reproduce the configuration in which two leads connect both ends of the Co line to a power supply. As long as $V_1 > V_2$ any value can be used to produce the same distribution of potential and current (we used $V_1 = 0$ and $V_2 = 1$). Once the distribution of potential V is found, the current distribution can be obtained with the relation $\vec{j} \propto \vec{\nabla} V$. We are interested only in the relative distribution of amplitudes, and the local directions of current. AMR is calculated at every cell as: $\Delta R_i = \cos^2(\theta)$, being θ the relative angle of the vectors $\vec{m}$ and $\vec{j}$ at each simulation cell. To compute the total distribution, it is necessary to weigh the contribution of each cell to the total AMR. To do this, the relative values of amplitude of current can be used, assuming that the ohmic resistance of the line is uniform: $\Delta R = \sum_i |\vec{j}_i| \times \Delta R_i$. In figure 11a) we show a calculated AMR curve corresponding to a single strip with width $w = 10$ μm and length $l = 2$ mm, with magnetic field applied perpendicular to it. As expected, at low fields the magnetization starts to rotate and, since current is applied parallel to the strip, AMR increases (the perpendicular orientation of $\vec{m}$ with respect to $\vec{j}$ yields the lowest AMR possible value).

It is difficult to know exactly some of the parameters of the Co line, such as the exchange stiffness. This can produce different results than expected from the measurements. For example, the simulations show an almost zero remanent field. To solve this problem, one can introduce artificially a distribution of uniaxial anisotropy, pointing in a random direction at every simulation cell, to account for the polycrystalline structure of the line grown by sputtering. The anisotropy constant can be adjusted, so that the remanent field matches that of the measurements. In this case a value of $K = 7 \times 10^4$ J/m^3 is enough (see Fig. 11 b)).

Simulated photocurrent distribution

To determine the AMR response of the photocurrents generated by the laser, we have focused on the case of a stationary current distribution. In this case, the diffusion equation for electrons reduces to Laplace's equation

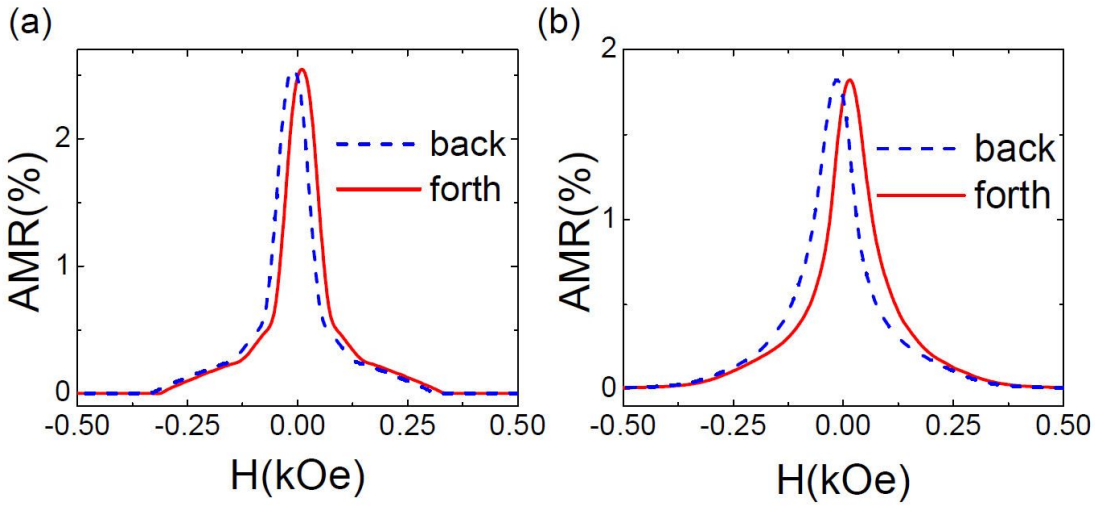

Figure 11. a) Simulated AMR of a stripline with field applied perpendicular to the line. b) The same simulation, including an artificial cell-wise random anisotropy.

again. Our approximate approach assumes that before applying the laser on the line, the potential was uniform in it (V_1). Once the laser is incident on the line, it takes the electron distribution out of equilibrium and the area receiving the laser excitation acts as a source of electrons that diffuse away from it, establishing a potential V_2 in this area (see Fig. 12 b)). Obviously, with this approach, the recombination of electrons and holes is not considered. We only use it to find the direction of the generated photocurrents.

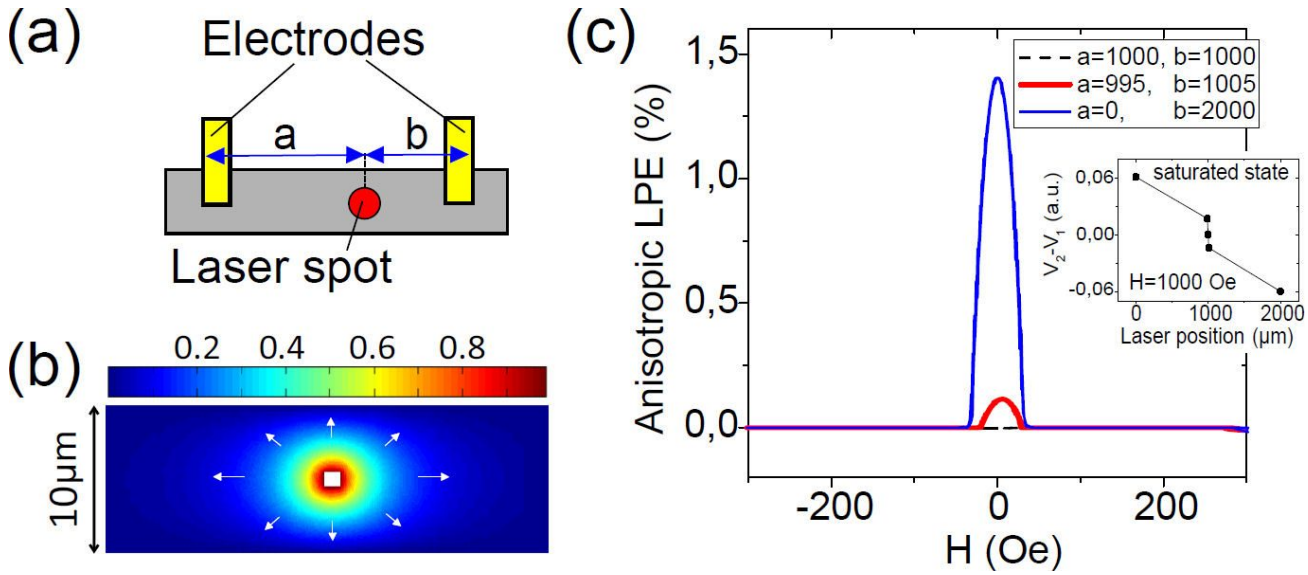

Figure 12. a) Sketch of the simulated system. b) Calculated stationary distribution of potential (colors, a.u.) and current (white arrows) generated by the laser (white square). c) Simulated increase in signal due to LPE. The inset shows the dependence of the offset signal at saturation as a function of laser position.

Once the current distribution is obtained, it is possible to calculate the contribution of AMR to the measured voltage between two electrodes. The calculation is as follows: given the current distribution at each simulation cell, a voltage drop can be assigned to it (the one responsible for that local current), in x and y directions. Because we place the electrodes across the line, the relevant direction is along the line. Therefore, the cells in the direction

perpendicular to the line will be averaged. The voltage drop due to AMR in each cell is given by $V_i = |j_i| \times \Delta R_i$. The voltage drop between the electrodes can be calculated by summing the local voltage drops from the laser to each single electrode and then taking the difference. We observe that although the calculated A-T-LPE is similar to the calculated AMR, its maximum value is somewhat lower and appears more abruptly at low magnetic fields where magnetization starts to rotate. As mentioned above, it is possible to introduce an artificial random anisotropy to reproduce the AMR curves more accurately. However, the magnetization distribution at low fields does not produce correct results of voltage drop between terminals in the case of photocurrents generated by the laser. This is due to the high disorder that appears at low fields, that is propagated and amplificated by the AMR formula, producing several random spikes. In this work we will focus only on results without anisotropy, to try to understand the nature of the measured signal. In figure 12 c) we show the calculated LPE vs field signal due to the AMR contribution. Even with the laser right in between the two electrodes, the signal is non zero, as it should. This is because the current distribution, due to the finite elements scheme, is not perfectly symmetric at both sides of the laser, and the slightest difference in potential at the electrodes is noticeable.

8. DISCUSSION AND CONCLUSIONS

To sum up, we have carried out a detailed investigation of the lateral photovoltaic effects in 5 to 20 micron wide $Co/SiO_2/Si$ line structures using two different experimental methods: time dependent studies with microsecond resolution and a lock-in technique (first harmonic amplitude and phase responses), completed by numerical analysis (Poisson equation with input from micromagnetic simulations and finite element analysis using ATLAS). We have presented evidence for new unexpected features of the LPE some of which are related with the narrow width of the Co line (inducing a qualitative change in the response due to the finite inductance of the line) while other features are related to the magnetic properties of the Cobalt (through change of its magnetic allignment with respect to the charge carriers drift velocity).

First of all (i) we observe experimentally, and confirm by fitting to the model of analytical theory, that T-LPE in thin line structures has a sign inversion after the laser is turned off, followed by a nearly exponential relaxation back to equilibrium. This unexpected behaviour has been explained by the influence of a local inductance of the Cobalt line structure,[23] in addition to a corresponding local capacitance and resistance which were previously, the only factors considered for wider LPE devices.

Secondly (ii), and following our former announcement in the abstract submitted in July 2014 to SPIE Photonics-West 2015 conference, we present a detailed experimental study of the influence of the magnetic state of the Cobalt overlayer on the transient LPE. The real time response analysis of the T-LPE shows about $0.3 - 0.6\%$ enhancement of LPE at small fields which is linked to changes in the anisotropic magnetoresistance (Fig. 6,7,11,12). We note that similar effects (but in the persistent illumination conditions and and for much wider ($\sim$mm) Permalloy films grown over SiO_2/Si have been very recently reported by Wang et al.[27] An important distinction of our experimental configuration is that in our case the transient LPE response to a few kHz laser pulse frequency is determined by the line inductance, capacitance and resistance (see above and[23]). Therefore, we believe that this makes our experimental method almost insensitive to the slowly changing potential difference developed on the surface of the Si aparted from the ferromagnetic structures. We are therefore confident that we observe an intrinsic T-LPE in narrow ferromagnetic line structures in MOS hybrids.

Our lock-in experiments (similary to what was previously observed in wide planar films[9,24]) confirm a clear correspondence between the phase response in the periodically driven LPE and the laser spot position along the line (see Fig. 9). Interestingly, by compensation of the LPE magnitude and phase in each spatial point along the Co line structure in the the presence of large saturation magnetic field (about 2 kOe), we were able to observe the dependence of the phase as a function of the Co magnetization direction relative to the drift velocity of the relaxing photo-carriers. We oserved an abrupt variation of the phase with the inversion of the magnetization direction, which has been explained with a simple model considering the inversion of the direction of Lorentz force acting on drifting photo-carriers as a consequence of the inversion of the Co magnetization (see the sketch in Fig. 8(b) explaining the effect in Figure 9(b)). Independent experimental studies involving analysis of the influence of magnetization direction on the characteristic relaxation (back to equilibrium) time shown on Figure 8(a) support the above simplified model.

In conclusion, we report on specific features of the Transient Lateral Photovoltaic Effect in micron sized patterned Ferromagnet/Insulator/Semiconductor structures. Besides, we observe an intrinsic anisotropic transient lateral photovoltaic effect in the presence of an external magnetic field. Further studies should provide details of the A-T-LPE in the longitudinal field geometry. We expect that our findings could stimulate the development of magnetically tuned micron-sized PSDs with an unmatched time-space resolution.

ACKNOWLEDGMENTS

We would like to acknowledge Jose Rodrigo and Laura Martín for their help at the initial stage of the experiment as well as Ch. van Haesendonk for the growth of the samples and Arkadi Levanyuk for discussions. We also acknowledge the support by the Spanish MINECO (MAT2012-32743), and the Comunidad de Madrid through NANOFRONTMAG-CM (S2013/MIT-2850) and CCC-UAM (SVORTEX).

REFERENCES

1. J. Wallmark, "A new semiconductor photocell using lateral photoeffect," *Proceedings of the IRE* **45**, pp. 474–483, 1957.
2. G. Lucovsky, "Photoeffects in nonuniformly irradiated pn junctions," *Journal of Applied Physics* **31**(6), pp. 1088–1095, 1960.
3. D. W. Boeringer and R. Tsu, "Lateral photovoltaic effect in porous silicon," *Applied Physics Letters* **65**(18), pp. 2332–2334, 1994.
4. K. Zhao, K.-j. Jin, H. Lu, Y. Huang, Q. Zhou, M. He, Z. Chen, Y. Zhou, and G. Yang, "Transient lateral photovoltaic effect in p-n heterojunctions of la0.7sr0.3mno3 and si," *Applied Physics Letters* **88**(14), p. 141914, 2006.
5. D. Kabra, T. B. Singh, and K. S. Narayan, "Semiconducting-polymer-based position-sensitive detectors," *Applied Physics Letters* **85**(21), pp. 5073–5075, 2004.
6. R. H. Willens, "Photoelectronic and electronic properties of ti/si amorphous superlattices," *Applied Physics Letters* **49**(11), pp. 663–665, 1986.
7. N. Tabatabaie, M. Meynadier, R. E. Nahory, J. P. Harbison, and L. T. Florez, "Large lateral photovoltaic effect in modulationdoped algaas/gaas heterostructures," *Applied Physics Letters* **55**(8), pp. 792–794, 1989.
8. H. van Zalinge, B. Özyilmaz, A. Böhm, R. W. van der Heijden, J. H. Wolter, and P. Wyder, "Observation of the screening signature in the lateral photovoltage of electrons in the quantum hall regime," *Phys. Rev. B* **64**, p. 235303, 2001.
9. H. Niu, C. Aoki, T. Matsuda, M. Takai, and M. Maeda, "A position-sensitive mos device using lateral photovoltaic effect," *Japanese Journal of Applied Physics* **26**(1A), p. L35, 1987.
10. C. Yu and H. Wang, "Large lateral photovoltaic effect in metal-(oxide-)semiconductor structures," *Sensors* **10**(11), pp. 10155–10180, 2010.
11. W. Jin, S. Zhang, H. Ni, W. Xiang, J. Xi, X. Feng, and K. Zhao, "Near infrared lateral photovoltaic effect in latio 3 films," *International Journal of Photoenergy* **2013**, 2013.
12. S. Q. Xiao, H. Wang, Z. C. Zhao, Y. Z. Gu, Y. X. Xia, and Z. H. Wang, "The Co-film-thickness dependent lateral photoeffect in Co-SiO2-Si metal-oxide-semiconductor structures," *Opt. Express* **16**, pp. 3798–3806, 2008.
13. H. Wang, S. Q. Xiao, C. Q. Yu, Y. X. Xia, Q. Y. Jin, and Z. H. Wang, "Correlation of magnetoresistance and lateral photovoltage in co 3 mn 2 o/sio 2 /si metal/oxide/semiconductor structure," *New Journal of Physics* **10**(9), p. 093006, 2008.
14. S. Q. Xiao, H. Wang, Z. C. Zhao, Y. Z. Gu, Y. X. Xia, and Z. H. Wang, "Lateral photovoltaic effect and magnetoresistance observed in cosio 2 si metaloxidesemiconductor structures," *Journal of Physics D: Applied Physics* **40**(22), p. 6926, 2007.
15. L. Kong, H. Wang, S. Xiao, J. Lu, Y. Xia, G. Hu, N. Dai, and Z. Wang, "Integrated properties of large lateral photovoltage and positive magnetoresistance in co/mn/co/c-si structures," *Journal of Physics D: Applied Physics* **41**(5), p. 052003, 2008.
16. C. Q. Yu and H. Wang, "Large near-infrared lateral photovoltaic effect observed in co/si metal-semiconductor structures," *Applied Physics Letters* **96**(17), p. 171102, 2010.

17. L. Kronik and Y. Shapira, "Surface photovoltage phenomena: theory, experiment, and applications," *Surface Science Reports* **37**(1-5), pp. 1 – 206, 1999.
18. D. Kabra, J. Verma, N. Vidhyadhiraja, and K. Narayan, "Model for studies of lateral photovoltaic effect in polymeric semiconductors," *Sensors Journal, IEEE* **8**, pp. 1663–1671, 2008.
19. S. Brems, K. Temst, and C. Van Haesendonck, "Origin of the training effect and asymmetry of the magnetization in polycrystalline exchange bias systems," *Phys. Rev. Lett.* **99**, p. 067201, 2007.
20. D. Herranz, R. Guerrero, R. Villar, F. G. Aliev, A. C. Swaving, R. A. Duine, C. van Haesendonck, and I. Vavra, "Anomalous low-frequency noise in synthetic antiferromagnets: Possible evidence of current-induced domain-wall motion," *Phys. Rev. B* **79**, p. 134423, 2009.
21. S. R. Dhariwal, L. S. Kothari, and S. C. Jain, "Transients in p-n-junction solar cells," *Journal of Physics D: Applied Physics* **9**(4), p. 631, 1976.
22. M. Vieira, "Speed photodetectors based on amorphous and microcrystalline silicon pin devices," *Applied Physics Letters* **70**(2), pp. 220–222, 1997.
23. J. P. Cascales, I. Martinez, D. Diaz, J. A. Rodrigo, and F. G. Aliev, "Transient lateral photovoltaic effect in patterned metal-oxide-semiconductor films," *Applied Physics Letters* **104**(23), p. 231118, 2014.
24. H. Niu, M. Maeda, Y. Matsubara, H. Yoshida, T. Matsuda, and S. Kishino, "An mos-type two-dimensional psd using the ac photovoltage phase," *Japanese Journal of Applied Physics* **28**(11R), p. 2206, 1989.
25. M. Donahue and D. Porter, "Oommf user's guide, version 1.0," 1999.
26. D. Grujicic and B. Pesic, "Micromagnetic studies of cobalt microbars fabricated by nanoimprint lithography and electrodeposition," *Journal of Magnetism and Magnetic Materials* **285**(3), pp. 303 – 313, 2005.
27. S. Wang, W. Wang, L. Zou, X. Zhang, J. Cai, Z. Sun, B. Shen, and J. Sun, "Magnetic tuning of the photovoltaic effect in silicon-based schottky junctions," *Advanced Materials* **26**(47), pp. 8059–8064, 2014.